14th Hypervelocity Impact Symposium 2017, HVIS2017, 24-28 April 2017, Canterbury, Kent, UK

Orion exploration flight test post-flight inspection and analysis

Miller, J. E.[a], Berger, E. L.[b], Bohl, W. E.[c], Christiansen, E. L.[d], Davis, B. A.[e], Deighton, K. D.[c], Enriquez, P. A.[a], Garcia, M. A.[a], Hyde, J. L.[f], and Oliveras, O. M.[b]*

[a]University of Texas at El Paso, 500 W. University Ave., El Paso, TX 79968
[b]Geo Control Systems Inc., NASA Johnson Space Center JETS contract, 2224 Bay Area Blvd., Houston, TX 77058
[c]Lockheed Martin Space Systems Company, 12257 S. Wadsworth Blvd., Denver, CO 80125
[d]NASA Johnson Space Center, 1101 NASA Rd. 1, Houston, TX 77058
[e]Jacobs, NASA Johnson Space Center JETS contract, 2224 Bay Area Blvd, Houston, TX 77058
[f]Barrios Technology Inc., NASA Johnson Space Center JETS contract, 2224 Bay Area Blvd, Houston, TX 77058

Abstract

The principal mechanism for developing orbital debris environment models, is to make observations of larger pieces of debris in the range of several centimeters and greater using radar and optical techniques. For particles that are smaller than this threshold, breakup and migration models of particles to returned surfaces in lower orbit are relied upon to quantify the flux. This reliance on models to derive spatial densities of particles that are of critical importance to spacecraft make the unique nature of the EFT-1's return surface a valuable metric. To this end detailed post-flight inspections have been performed of the returned EFT-1 backshell, and the inspections identified six candidate impact sites that were not present during the pre-flight inspections. This paper describes the post-flight analysis efforts to characterize the EFT-1 mission craters. This effort included ground based testing to understand small particle impact craters in the thermal protection material, the pre- and post-flight inspection, the crater analysis using optical, X-ray computed tomography (CT) and scanning electron microscope (SEM) techniques, and numerical simulations.
© 2017 The Authors. Published by Elsevier Ltd.
Peer-review under responsibility of the scientific committee of the 14th Hypervelocity Impact Symposium 2017.

Keywords: Orion; Exploration Flight Test; Orbital Debris

---

* Corresponding author. Tel.: +01-281-244-8093.
  E-mail address: joshua.e.miller@nasa.gov

1. Introduction

The multipurpose crew vehicle, Orion, is being designed and built for NASA to handle the rigors of crew launch, sustainment and return from scientific missions beyond Earth orbit [1]. In this role, the Orion vehicle is meant to operate in the space environments, like the meteoroid and the orbital debris environments (MMOD), with successful atmospheric reentry after the flight [2]. To accomplish this role, the exposed surfaces of Orion's reentry module uses durable, porous-ceramic tiles on almost thirty square meters of the conical section that protects the crew. These durable, non-ablative surfaces maintain their surface profile through atmospheric reentry; thus, they preserve any surface imperfections that occur prior to atmospheric reentry [3]. Furthermore, Orion's launch abort system includes a shroud that protects the thermal protection system while awaiting launch and during ascent. The combination of these design features and a careful pre-flight inspection to identify any manufacturing imperfections results in a high confidence that damage to the thermal protection system identified post-flight is due to the in-flight environments.

The first exploration flight test mission, EFT-1, took the Orion reentry vehicle through two orbits of the Earth with the first orbit achieving an apogee of approximately 1,000 km and a second orbit apogee of just under 6,000 km as illustrated by the blue flight profile curve in Fig. 1 [4]. This flight profile took Orion beyond the inner Van Allen radiation belts and had a very high reentry speed. These features represent a realistic, stressing conditions for the vehicle from the natural environment; however, the radiation and energetic reentry were not the only stressing conditions experienced by Orion on this test flight. Because EFT-1 spent a significant fraction of time in some of the worst bands of orbital debris the mission also represented a unique observation of the orbital debris environment.

The predicted orbital debris environment from the recently developed NASA orbital debris engineering model, ORDEM3.0, is also shown in Fig. 1 as a black curve where the flux of 1 mm solid particles and greater at a given altitude are normalized to the flux at 400 km [5]. The flux at 400 km is representative of the operational environment of the International Space Station where most of the previous returned surfaces originated. As can be seen, the predicted flux on the reentry vehicle approached thirty-five times that at the ISS near the apogee of the first orbit, which EFT-1 visited two more times on the second orbit. This EFT-1 trajectory coupled with the architecture of Orion results in the first ever direct measurements of the worst debris bands surrounding Earth from a large returned surface.
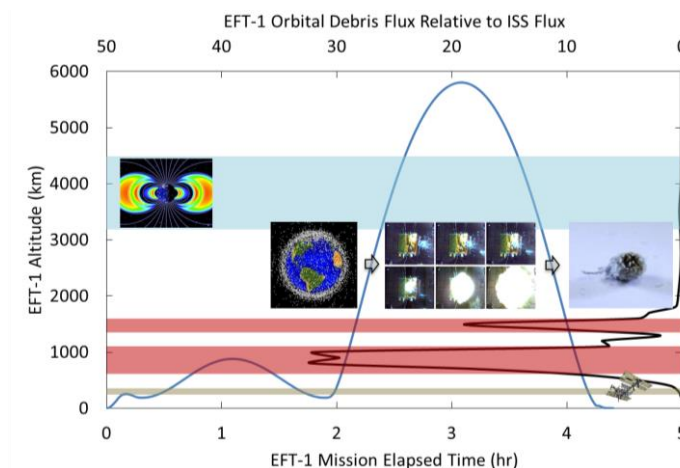

Fig. 1. Orion's EFT-1 flight profile (blue curve) relative to debris environment (black curve).

2. Ground based impact experiments

In preparation to support the flight inspection and to inform the analysis after the flight, impact experiments using the two-stage, light-gas, guns of the NASA White Sands Test Facility in Las Cruces, New Mexico have been performed. These impact experiments informed the inspectors to the type of damage and impact remnants that are present from sub-millimeter particle impacts. The combined results from the work are summarized in Table 1. For

each of the experiments, the particle material, size and the impact speed and obliquity relative to the tile surface normal are given along with the damage measurements. The damage measurements have been obtained from computed tomography (CT) scans using North Star Imaging software and a custom system that uses a Hamamatsu 150kV Microfocus L8121-03 source with a PerkinElmer XRD 1621detector. A representative profile is shown in Fig. 2a. As can be seen, sub-0.1 mm or low density particles are required for 1 mm or less penetration depth.

Table 1. Impact experiment summary for Orion EFT-1.

Test	Projectile		Impact		Damage	
	Material	Diameter (mm)	Speed (km/s)	Obliquity (°)	Entrance (mm x mm)	Depth (mm)
HITF14233	Al	0.3	7.13	45	2.5 x 2.7	2.25
HITF14235	Al_2O_3	0.2	7.05	45	1.2 x 0.8	1.8
HITF14237	Steel	0.25	6.97	45	3.0 x 2.5	3.8
HITF16072[*]	Glass	0.1	7.0	0	0.35±0.05	0.79±0.19

[*]Test used multiple spheres in a single shot, thus the experiment yielded average values

In addition to providing comparison craters for the post-flight inspection, the ground based impact experiments also provide ballistic information for the extrapolation of damage observations to probable particle size as shown in Fig. 2b. The experiments are modeled assuming surface coating properties of an average density of 0.45 g/cm³, an average strength of 2 MPa and a shock wave speed that is 1.3 times the particle speed [6]. The solid lines in the figure are the particle sizes to achieve the depth of penetration as a function of the impact speed for each of the experiments.

a)

b)
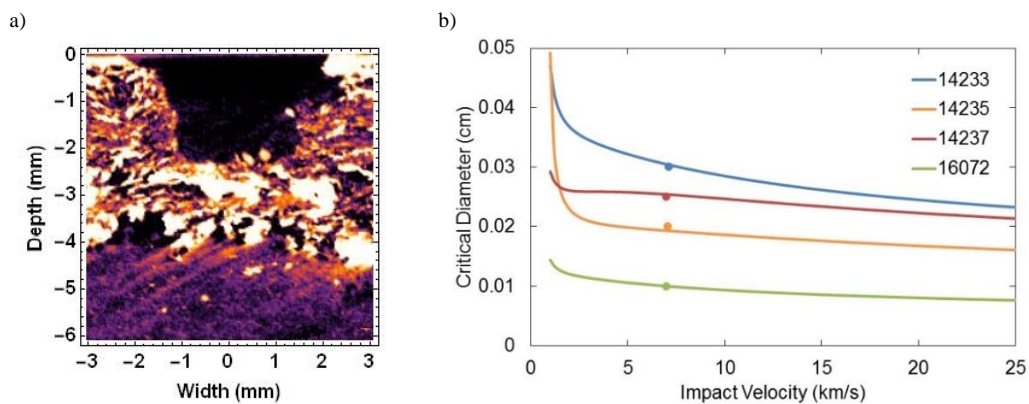
expeFig. 2. Impact experiments performed to determine penetration depth a) from crater profiles measured by CT-scans like that from HITF14233 and b) the comparison of experiments to the ballistic model.

3. Flight vehicle inspections

After the Orion thermal protection system was assembled, but prior to the mating of the Orion crew module to the service module, a detailed preflight inspection was performed on the backshell thermal protection tiles. This phase of the inspection identified any visible features and produced photographs that had at least four pixels over every square millimeter of the backshell to serve as a reference for post-flight analysis. Immediately following these final inspections, the crew module was fueled and mated before departing for the Cape Canaveral launch pad.

Six minutes after launch, the launch abort system jettisoned from the Orion crew module exposing the backshell to the near-Earth environments. The upper stage placed Orion in an attitude where the Orion central axis was broadside to the velocity vector and rotated about the central axis for thermal conditioning. This vehicle attitude was used during each passage of the debris bands except the last where the service module and upper stage separated from the crew module. The crew module reoriented itself for atmospheric entry with the heatshield forward. A little over four hours later the crew module splashed down in the Pacific Ocean off the coast of Baja California.

Orion was recovered by the USS Anchorage 630 statute miles south of San Diego. NASA and Lockheed Martin inspection personnel were on board the ship and performed an initial assessment of the backshell from the well deck while *en route* to Naval Base San Diego. At the base, an initial detailed inspection identified and protected eight regions of interest prior to the trip back to the Kennedy Space Center (KSC). After arrival at KSC two additional detailed inspections were also performed before and after the backshell panels were removed from the vehicle.

In all twenty-five regions of interest (ROI) have been identified by the three post flight inspections. These regions of interest have been compared to the preflight imagery and five candidate impact sites were selected for removal from the vehicle for detailed analysis. A sixth candidate impact site has also been identified; however, due to its location on the vehicle, it is not available for detailed analysis. The candidate impact sites, there location on the vehicle, and optical damage measurements from an 8400K Digital Optical Micrometer are shown in Fig. 3.
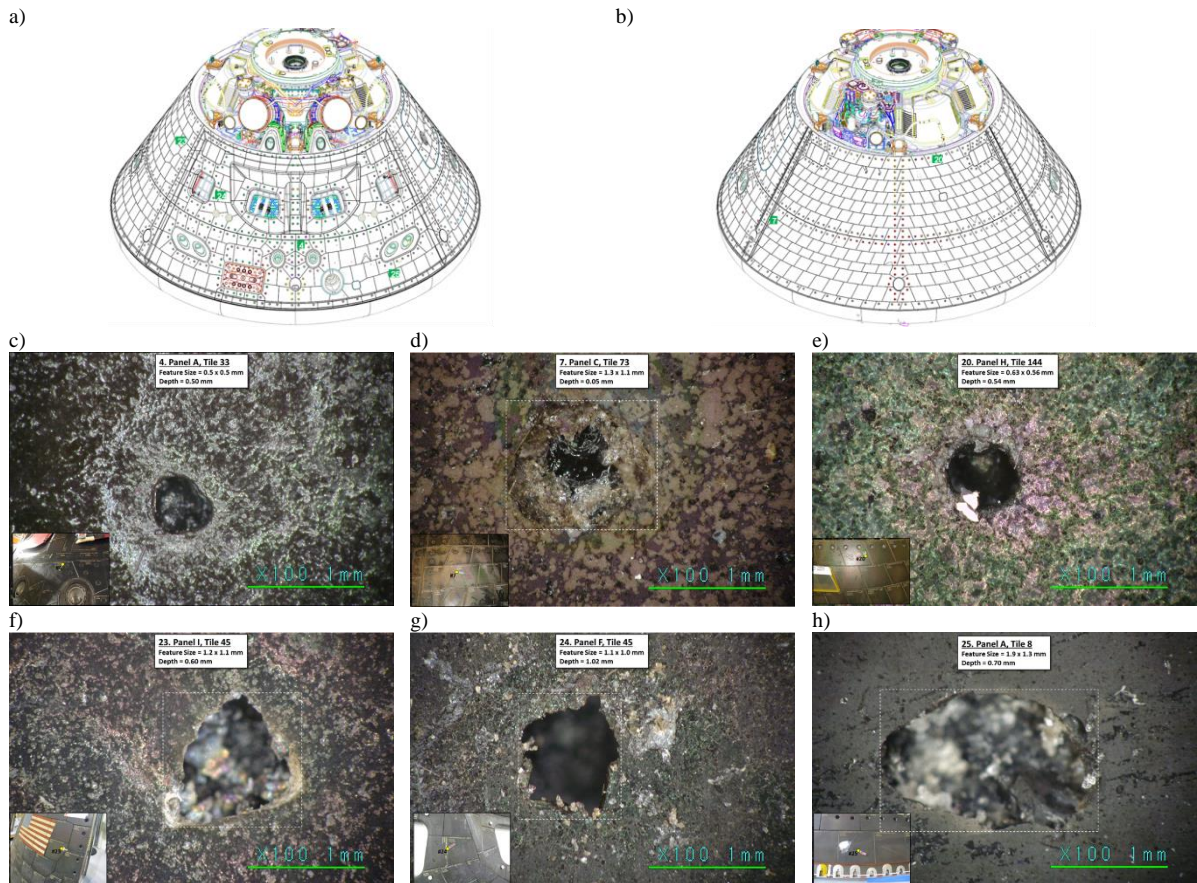

Fig. 3. Six candidate impact craters from EFT-1 post-flight inspection a) location on the heads side of the capsule and b) seats side of the capsule with close-up and inset general view of c) ROI4, d) ROI7, e) ROI20, f) ROI23, g) ROI24 and h) ROI25.

4. X-ray CT evaluation

The five tiles that contained the regions of interest 4, 7, 20, 24 and 25 have been removed from their Orion backshell carrier panels for detailed analysis. The tile surrounding the craters has been removed leaving approximately 1 cm cubes surrounding the craters. These craters have also been CT-scanned for crater profiles with the crater volume and cross-sectional profiles along the major axis and the minor axis shown in Fig. 4 except for ROI7. Due to the shallowness of ROI 7, those scans have not been reproduced here.
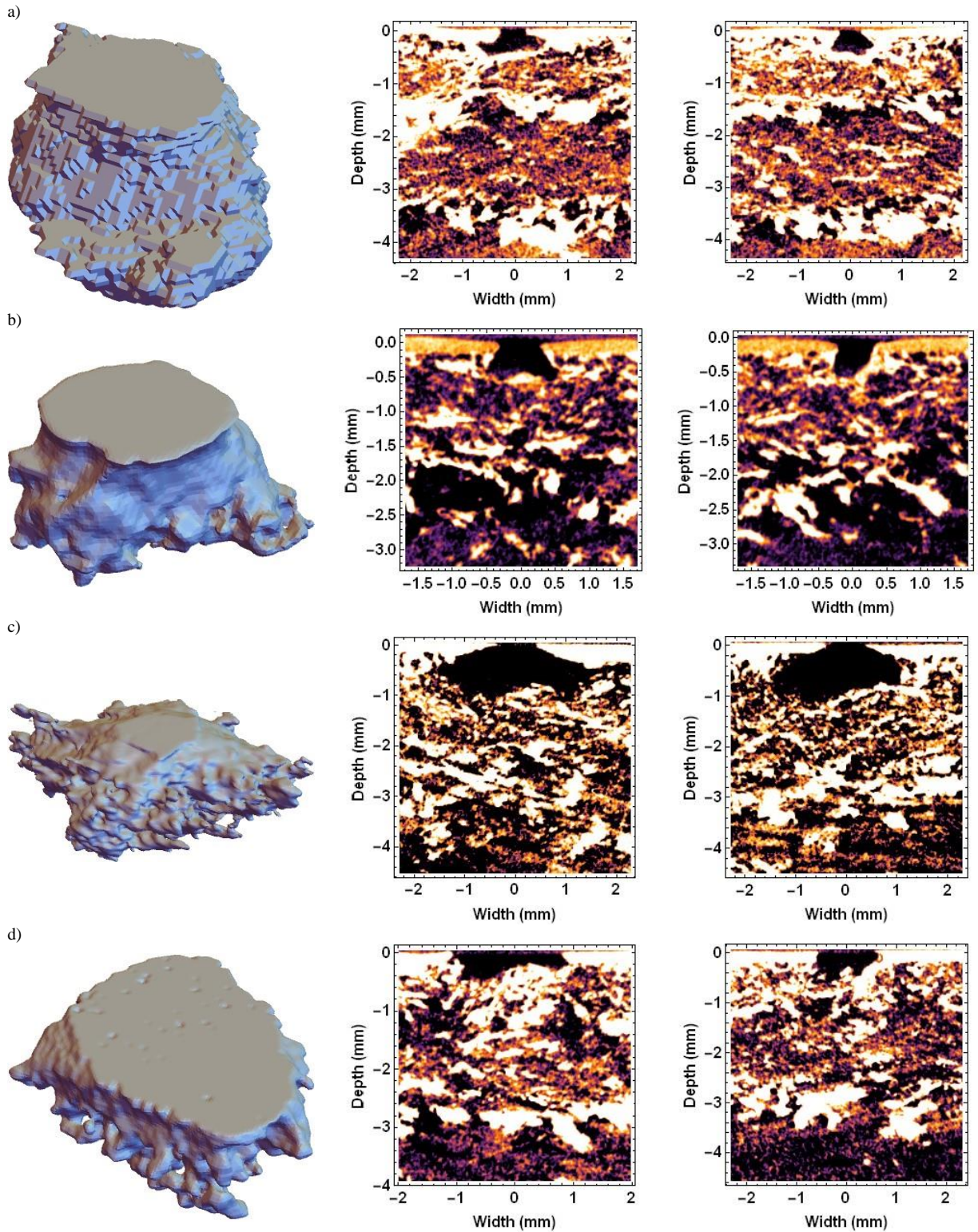
a)

b)

c)

d)

Fig. 4. CT-scan volume, major axis profile and minor axis profile for a) ROI4, b) ROI20, c) ROI24 and d) ROI25.

5. SEM evaluation

After detailed analysis of the available candidate impact craters using both optical and X-ray techniques, scanning electron microscope (SEM) data has also been collected from the surface as well as from machined cross-sections of each crater. Prior to machining, the candidate craters and surrounding porous material has been filled with epoxy using a vacuum drawing technique and then hardened. The hardened sample has then been cut using a diamond lathe to expose areas identified by the non-destructive CT-scans. Three to four cross-sections from each candidate crater have been analyzed and at least one section from each candidate crossed near the center of the crater.

Each freshly exposed cross-sectional surface has been carbon-coated and analyzed using a JEOL JSM-7600F Field Emission Scanning Electron Microscope (SEM), which is equipped with two secondary electron detectors (in-lens and in-chamber), an in-lens backscattered electron detector for short working distances, and a low-angle in-chamber backscattered electron detector. The SEM is also equipped with a Thermo Scientific energy-dispersive X-ray (EDX) spectrometer, allowing for rapid acquisition of compositional information and element maps from regions of interest. Back-scattered electron (BSE) images, like that shown in Fig. 5a, and X-ray mosaic maps (for all elements, excepting H, Li and B), Fig. 5b, have been collected at 150x over areas surrounding the candidate craters in each slice. These data have been used to identify regions with possible impactor residue, i.e., those that contained sub-micron-sized or larger pieces of foreign material like that shown in Fig. 5c.
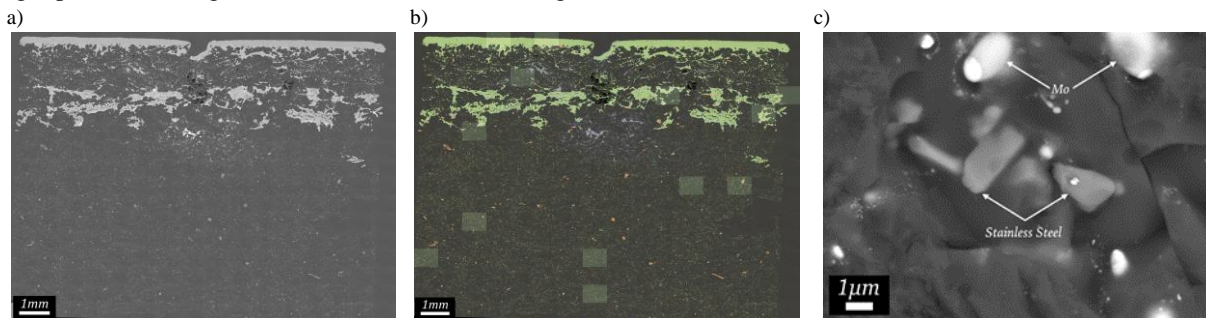

Fig. 5. Representative SEM data from a cross-section of ROI20 from near the middle of the crater a) BSE map, b) False-color X-ray maps superimposed on the BSE map (Al=red, Si=green, Mo=blue) highlighting AETB material, and c) stainless steel fragments, embedded in AETB (gray material). The molybdenum (bright white material) exhibits a melt texture surrounding the larger molybdenum pieces.

Both textural and compositional information have been used to examine possible impactor residue. Due to the composition of the tile's surface coatings (Al, Si, Mo) and epoxy components (C, Cl) some materials are difficult to identify against the background materials (e.g., pure silica, certain aluminum alloys and plastics). Some examples of identified foreign materials include: stainless steel (Fe, Cr, Mn), bronze (Cu, Sn), meteoritic assemblages (mixtures of silicate minerals, Fe-Ni-metal, Fe-Ni-sulfides, Fe-oxide, chromite, and ilmenite), and salts (e.g., NaCl) attributable to seawater exposure. The significant findings from this investigation are summarized in Table 2.

6. Numerical investigations

With the crater morphology and estimates of candidate materials, impact simulations have been performed to narrow down shapes and impact orientations that might have created the craters. To perform these simulations, the three-dimensional, non-linear, structural dynamics tool CTH has been used. The simulations modeled the outermost surface coatings of the backshell tiles to 1 cm in all directions from the impact point adjusted to keep the oblique impact crater within the model space. This model space has been broken up into cubic elements of 20 µm.

For the surface coating materials, the SESAME 7360 model for silica with multiple layers representing a decrease from an amorphous glass to the highly porous tile has been used. This has been accomplished using the P-alpha model for porosity, with the outer most layer modeled as 0.1 mm thick with a density of 2.2 g/cm^3. The subsequent layers are similarly modeled with 0.15 mm of 1.5 g/cm^3, 2.55 mm of 0.45 g/cm^3, and 2 mm of 0.128 g/cm^3. The remainder of the tile is modeled as a sound absorbing (semi-infinite) boundary condition. Full compaction strengths for the layers

have been modeled at 41, 28, 8 and 2 MPa. Similarly, the tensile strengths for the layers have been modeled at 14, 9, 3 and 0.8 MPa.

Table 2. Significant SEM findings.

Sample	Summary
ROI4	There are multiple regions of nanometer-scale, Fe-oxide particles mixed with AETB material and salts along a trail and in additional multiple discrete regions of the cross-section of the crater. These regions also contain minor Ca and Mg, which may be attributed to salt or silicate mineral contributions. Fe-oxide and Cr (possible chromite) with associated melt droplets of molybdenum, are found near the crater rim, and meteoritic assemblages have also been found.
ROI7	The crater is infilled with a highly-specular glass material and there is no evidence of salt within the sections indicating that infill occurred prior to sea water exposure. Iron and AETB components are intermixed/melted together. There are meteoritic assemblages on one cross-section.
ROI20	One cross-section includes a trail of Fe- and Cr-rich material (stainless steel) intermixed with AETB. This material is co-located along the same trajectory as salts. Textural evidence for melting and rapid cooling (e.g., impact event) is shown in figure X; Associated with stainless steel fragments are micron-sized pieces of molybdenum surrounded by nm-scale molybdenum melt droplets.
ROI24	There is no textural evidence for impactor residue on any of the sections; however, assemblages of meteoritic material have been found in one cross-section.
ROI25	Cu- and Sn-rich material (bronze) and Fe- and Cr-rich material (stainless steel) have been found intermixed/melted with AETB material. The bronze is found concentrically surrounding crater. Stainless steel is found nearer to the crater and along the crater rim in the second slice.

Projectile models used native material models of CTH. For these simulations, high density materials have been modeled as iron, medium density as carbon, and low density as polyamide. Meteoritic simulations assume that the likely material is cometary dust and uses various porosities of ice to represent these impactors. In all cases SESAME models are used so that variable thermodynamic properties are addressed. The projectiles considered included spheres for chunks and cylinders of various dimensions to cover flakes through fibers. The projectiles have been varied in impact velocity relative to the tile surface normal and rotated the central axis of the cylinders about its center to account for the pitch of the projectile. While this study has an infinite range of potential impact conditions, Table 3 summarizes the impact conditions that have been found to most closely reproduce the craters from this analysis.

Table 3. Simulation findings.

Sample	Summary
ROI4	Simulations have found that a medium density, cylindrical projectile (30 μm diameter x 300 μm length) that impacts normal to the tile surface at 12 km/s with the cylinder axis perpendicular to the velocity vector best models the crater.
ROI7	Simulations have found that a porous ice (0.1 g/cm^3) spherical projectile (500 μm diameter) that impacts 45° to normal of the tile surface at about 25 km/s best models the crater.
ROI20	Simulations have found that a high density, cylindrical projectile (180 μm diameter x 30 μm length) that impacts 45° to normal of the tile surface at 3 km/s with the cylinder axis rotated 75° to the velocity vector best models the crater.
ROI24	Simulations have found that a porous ice (0.1 g/cm^3) spherical projectile (1 mm diameter) that impacts normal to the tile surface at about 25 km/s best models the crater.
ROI25	Simulations have found that a high density, cylindrical projectile (180 μm diameter x 30 μm length) that impacts 65° to normal of the tile surface at 3 km/s with the cylinder axis rotated -20° to the velocity vector best models the crater.

7. Conclusions

The principal purpose of any post-flight inspection of a single use system like Orion is to understand the environment and to check that the environmental engineering models going into design decisions are reflective of reality. To accomplish this comparison, the BUMPER3 analysis code managed by NASA and used for MMOD analyses of many crewed and robotic missions has been selected for Orion. The BUMPER3 code sums the number of impacts over spacecraft surfaces based on trajectory and attitude within the meteoroid and orbital debris environment.

The model geometry for the EFT-1 Orion has been converted into a discretized surface model for use within BUMPER3. The rate of particles that cross each element are calculated from the product of the environmental flux and the projected area of the element from a threat direction, which is summed over all potential threat directions from

the background environment. In the case of the environment models used with BUMPER3 like the Orbital Debris Engineering Model version 3 (ORDEM 3.0)and the Meteoroid Engineering Model version 2 (MEM R2), the spectral flux has been integrated, so the term flux refers to a particle size and all larger particles defined by the ballistic model. The number of particles that cross the element is then integrated from the product of the calculated rate crossing the surface through the mission duration. For the final desired total number of impacts on a system, like the EFT-1 TPS, these elements are summed over the entire surface. In Fig. 6 the cumulative count for penetration to a specific depth for the EFT-1 backshell is shown by the curves. As can be seen from the curves, only a crater of a half millimeter or less is expected using ORDEM 3.0 and about a tenth of a millimeter or less is expected from MEM R2.
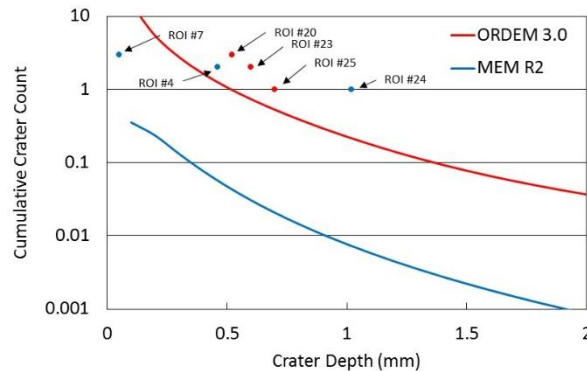

Fig. 6. Predicted cumulative count for orbital debris (red) and meteoroid (blue) environments currently used for Orion and the observed impacts.

The depths of penetration from the flight are graphed atop the analysis curves in Fig. 6 assuming all candidates are deemed to be in-flight impacts. Since the environment models have integrated the spectral flux of particles, the largest ROI found has been graphed as unity, the next smaller as two (that one plus one larger), and so on. In this figure, it has been assumed that ROI20, ROI23 and ROI25 resulted from orbital debris impacts, and it has been assumed that ROI4, ROI7 and ROI24 resulted from meteoroid impacts. Adjusting the origin of any of the craters has a corresponding adjustment in the figure, and as the analysis is still on-going, these are not considered final but representative findings.

Acknowledgements

References

[1] D. R. Sauvageau, J. B. Hopkins, K. Riley and T. Martin, Future SLS-Orion missions supporting evolution to Mars, *AIAA SPACE 2015*, AIAA-2015-4441 (2015).
[2] J. E. Miller, W. E. Bohl, E. L. Christiansen and B. A. Davis, Ballistic performance of porous-ceramic, thermal protection systems, *Int. J. Imp. Eng.* 56 (2012) 40-46.
[3] C. Sipe, and B. Hinde, Orion thermal protection system design development. *AIAA Space 2008*, AIAA-2008-7801 (2008).
[4] NASA, Orion Flight Test: Exploration Flight Test-1, Orion Flight Test: Exploration Flight Test-1, NP–2014–11–020–JSC (2014).
[5] P. H. Krisko, The new NASA Orbital Debris Engineering Model ORDEM 3.0, *AIAA/AAS Astrodynamics Specialist Conference*, AIAA 2014-4227 (2014).
[6] J. E. Miller, E. L. Christiansen, B. A. Davis, and K. D. Deighton, Ballistic performance model of crater formation in monolithic, porous thermal protection systems, *Procedia Engineering*, 103 (2015) 398-404.